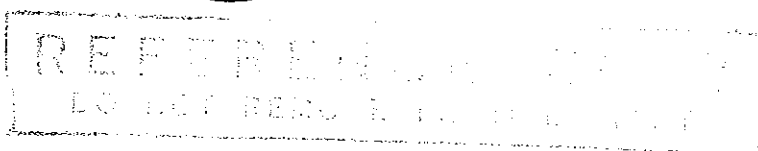


AAEC/E302

*Library*  
AAEC/E302



**AUSTRALIAN ATOMIC ENERGY COMMISSION**  
**RESEARCH ESTABLISHMENT**  
**LUCAS HEIGHTS**

**THE MEASUREMENT OF PARTIAL CAPTURE CROSS SECTIONS**  
**FOR NEUTRON ENERGIES ABOVE 10 keV**

by

G. J. BROOMHALL

M. J. KENNY

P. W. MARTIN \*

J. R. BIRD

\* Work carried out while on leave from University of British Columbia

May 1974

ISBN 0 642 99618 0



AUSTRALIAN ATOMIC ENERGY COMMISSION  
RESEARCH ESTABLISHMENT  
LUCAS HEIGHTS

THE MEASUREMENT OF PARTIAL CAPTURE CROSS SECTIONS FOR  
NEUTRON ENERGIES ABOVE 10 keV

by

G. J. BROOMHALL  
M. J. KENNY  
P. W. MARTIN\*  
J. R. BIRD

ABSTRACT

A large NaI detector has been used to demonstrate the feasibility of measuring partial capture cross sections for neutron energies from 10 to 100 keV. The pulsed neutron source was a 3 MeV accelerator and the  ${}^7\text{Li}(p,n)$  reaction with a time resolution of 3 to 4 ns and flight paths of 0.6 to 1.5 m. The experimental techniques are described, and illustrated by results for high energy transitions following capture in  ${}^{48}\text{Ti}$ ,  ${}^{56}\text{Fe}$ ,  ${}^{58}\text{Ni}$  and  ${}^{207}\text{Pb}$ .

\* Work carried out while on leave from University of British Columbia

National Library of Australia card number and ISBN 0 642 99618 0

The following descriptors have been selected from the INIS Thesaurus to describe the subject content of this report for information retrieval purposes. For further details please refer to IAEA-INIS-12 (INIS: Manual for Indexing) and IAEA-INIS-13 (INIS: Thesaurus) published in Vienna by the International Atomic Energy Agency.

CAPTURE; CROSS SECTIONS; ENERGY LEVELS; ENERGY-LEVEL TRANSITIONS;  
DATA PROCESSING; GAMMA DETECTION; GAMMA SPECTRA; IRON 56 TARGET;  
IRON 57; KEV RANGE 10-100; LEAD 207 TARGET; LEAD 208; NEUTRON REACTIONS;  
NICKEL 58 TARGET; NICKEL 59; PULSED NEUTRON TECHNIQUES; S WAVES;  
SHIELDING; SOLID SCINTILLATION DETECTORS; TITANIUM 48 TARGET;  
TITANIUM 49

## CONTENTS

	Page
1. INTRODUCTION	1
2. EXPERIMENTAL DETAILS	1
2.1 Detector Timing	1
2.2 Detector Response Functions	2
2.3 Shielding	2
2.4 Data Analysis	3
2.5 Normalisation	3
3. RESULTS AND DISCUSSION	3
3.1 Titanium	4
3.2 Iron	5
3.3 Nickel	5
3.4 Lead	5
4. CONCLUSIONS	6
5. REFERENCES	6

Table 1 Details of Target Materials and Running Conditions

Table 2 Resonances in  $^{48}\text{Ti}(n,\gamma)^{49}\text{Ti}$

Table 3 Resonances in  $^{56}\text{Fe}(n,\gamma)^{57}\text{Fe}$

Table 4 Resonances in  $^{58}\text{Ni}(n,\gamma)^{59}\text{Ni}$

Figure 1 Time resolution of prompt gamma peak for four pulse height ranges

Figure 2 NaI detector response functions for a 9.94 MeV gamma ray (F = full energy peak, S = single escape peak)

Figure 3 Detector shielding assembly (longitudinal section)

Figure 4 Relative partial capture cross sections for capture by  $^{47}\text{Ti}$  and  $^{48}\text{Ti}$  using a 1.00 m flight path for various pulse height intervals

Figure 5 Relative partial capture cross section for capture by  $^{48}\text{Ti}$  between 12 and 23 keV using 1.00 m flight path

Figure 6 Relative partial capture cross sections for capture by iron using a 1.50 m flight path for various pulse height intervals

Figure 7 Relative partial capture cross sections for capture by nickel using a 0.63 m flight path for various pulse height intervals

Figure 8 Capture cross section for the ground state transition following capture by  $^{207}\text{Pb}$  using a 1.00 m flight path



## 1. INTRODUCTION

The study of neutron capture for incident energies above 10 keV has always been difficult because of the combination of low cross sections and low neutron source strengths. High power electron linear accelerators have provided suitable neutron sources for capture cross section measurements (Allen and Macklin 1971) and detailed results are becoming available for most nuclei for neutron energies up to 100 keV and higher.

The study of individual gamma rays from neutron capture is still limited because the precision detectors required are affected by the gamma flash from electron 'linacs' and the lower neutron intensity from other sources.

This report presents results obtained with a NaI detector used with a  ${}^7\text{Li}(p,n)$  pulsed neutron source to obtain a time resolution of 2 to 4 ns/m. Further details are given by Broomhall (1972a). Individual gamma rays in Ti, Fe, Ni and Pb are observed and the neutron energy dependence of their intensities measured in the range 10 to 80 keV. These nuclei are characterised by the occurrence of a number of large, well-spaced s-wave resonances so it is possible to investigate the effects of level-level interference in partial capture cross sections.

## 2. EXPERIMENTAL DETAILS

Neutrons were produced using the  ${}^7\text{Li}(p,n)$  Be reaction. The proton source was the AAEC 3 MeV Van de Graaff accelerator, operating with a 2 ns klystron bunched beam at 1 MHz repetition rate and up to 8  $\mu\text{A}$  average current. For a proton energy 12 keV above threshold, neutrons with energies between 5 and 70 keV were produced in a forward cone, with the peak flux at 37 keV.

Thin samples were used to minimise multiple scattering effects and timing uncertainties due to target thickness. The targets were curved with a radius of curvature equal to the flight path length. Details of targets are summarised in Table 1.

Time of flight spectra were measured simultaneously for up to twelve different pulse height intervals using a PDP-7 on-line computer.

### 2.1 Detector Timing

Four matched RCA 8054 photomultipliers were used for light collection from the 20 cm x 15 cm NaI crystal. The outputs were summed and the signal was split into separate parts for timing and pulse height analysis. Timing signals were derived using a timing filter amplifier and a constant fraction discriminator.

Figure 1 shows the timing resolution as a function of  $\gamma$ -ray energy with pulse height intervals as for the nickel data reported in Section 3.3. For the pulse height range 8.0 to 8.7 MeV, the observed time resolution was 3.1 ns and for the range 2.4 to 7.3 MeV it was 4.0 ns. The beam pulse and the time pick-off, together with its associated electronics, gave a time resolution of 2.3 ns. Assuming that the detector and beam contributions are added in quadrature, the detector resolution for the restricted range was 2.1 ns and for the wider range it was 3.0 ns.

### 2.2 Detector Response Functions

The measured pulse height resolution of the detector was 8 per cent at 667 keV. In the region of interest (5 to 10 MeV), the response function of this crystal for monoenergetic  $\gamma$ -rays consisted of a full energy peak corresponding to the energy of the  $\gamma$ -ray, a single escape peak and a Compton tail. The ratios of full energy to single escape to tail vary with  $\gamma$ -ray energy. The response functions for 11 energies between 0.637 MeV and 17 MeV were measured using radioactive sources and discrete  $\gamma$ -rays from proton and neutron induced reactions. Figure 2

shows the response function for the 9.94 MeV  $\gamma$ -ray from the  $^{27}\text{Al}(p,\gamma)$  reaction (for both 10 cm and 20 cm diameter lead collimators).

### 2.3 Shielding

Gamma rays with energies up to 17 MeV are produced in the  $^7\text{Li}(p,\gamma)$  reaction. Even though they occur at zero flight time and serve as a useful time reference, they can cause an unnecessarily high dead time unless shielded out. Capture of neutrons by surrounding materials (e.g. reinforced concrete) gives rise to a spectrum of background  $\gamma$ -rays, both time dependent and time independent.

Neutrons reaching the detector can give rise to capture by either sodium or iodine. At kilovolt energies, sodium has a capture cross section of only 2.7 mb, but the capture product  $^{24}\text{Na}$  has a 15 hour life and decays with the release of a 2.74 MeV  $\gamma$ -ray. The iodine capture cross section is 760 mb and the summing of individual pulse heights following neutron capture in the iodine results in a pulse height spectrum corresponding to a 6.82 MeV  $\gamma$ -ray. Since this energy is close to the neutron binding energy for many nuclei, the detector must be adequately shielded from neutrons.

In designing an appropriate shield, the main considerations were to prevent direct and indirect neutrons from reaching the crystal and to minimise the number of background  $\gamma$ -rays penetrating the shield. The details of the shield have been given elsewhere (Broomhall 1971). The final configuration is shown in Figure 3. The relative amounts of shielding materials were chosen after using the neutron transport code SLABBO (Clancy 1969) to calculate transmissions through slabs of standard thickness. The region closest to the detector consisted of a 5 cm mixture of litharge ( $\text{PbO}$ ), glycerine ( $\text{C}_3\text{H}_8\text{O}_3$ ), boron carbide and lead shot in the weight ratios 5:1:4:10. Surrounding this was a 10 cm layer of antimony free lead, then 5 cm of boron carbide in paraffin and finally 20 cm of boric acid in paraffin wax. For the front face, 10 cm of boron carbide in paraffin wax was used. The total weight of the assembly was approximately 900 kg and it could be manoeuvred into position using a hover-pallet.

Use of this shield instead of a boric acid in paraffin wax shield gave an improvement of a factor of ten in peak to background ratio for gamma rays from the 37 keV titanium resonance. The floor and walls within 5 m of the target were covered with 10 cm of boric acid in paraffin wax. A large proportion of the remaining background was attributed to capture in iron and other structural materials in the experimental area.

### 2.4 Data Analysis

Results were accumulated as six blocks of 1024 channels or twelve blocks of 512 channels. One block was used to store the pulse height spectrum and the remainder were used to store time of flight spectra for preselected regions of  $\gamma$ -ray pulse height. At the end of each run the data were transferred via paper tape to disk files on an IBM 360 for processing and were subsequently stored on magnetic tape.

After each run, spectra were obtained using a cadmium sample of similar geometry. Background spectra were calculated and subtracted from both sample and cadmium runs. The sample spectra were then divided (channel by channel) by the cadmium spectra, thus correcting for the variation in neutron flux with energy.

For measurements on nuclei with a few well spaced gamma ray transitions, the preselected regions of pulse height were chosen so that simple corrections could be made to the counts in one region to obtain a relative partial cross section for one or a few gamma rays only. The appropriate correction factors were obtained from the known pulse height response functions of the NaI detector.

An alternative method of data collection and analysis would be to record a two-dimensional set of data points with a sufficient number of pulse height channels to permit least squares fitting of response functions to obtain estimates of the gamma ray intensities for each neutron time of flight channel. This method was not used in obtaining the results that follow because of the low count rates from the thin targets used.

## 2.5 Normalisation

Two methods are available for normalisation of the results to obtain absolute partial cross sections ( $\sigma_{\gamma ij}$ ). For thin targets these are:

### 1. The use of a resonance with known parameters

$$\sigma_{\gamma ij} = \frac{R_{ij}}{n} \cdot \frac{A_R}{A_{R'}} \cdot \frac{\epsilon_R}{\epsilon_i} \cdot \frac{a_R}{a_i}$$

where  $R_{ij}$  is the ratio of sample counts to cadmium counts in time of flight channel  $j$ ,

$n$  is the sample thickness (atoms  $\text{cm}^{-2}$ ),

$A_R, A_{R'}$  are the capture areas for the standard resonance as calculated from resonance parameters or as observed,

$\epsilon_i, a_i$  are the detection efficiency and gamma ray attenuation (in target, neutron shield and detector housing) for the  $i^{\text{th}}$  gamma ray, and

$\epsilon_R, a_R$  are the corresponding quantities for the gamma ray energies used for the standard resonance.

If the standard resonance is in a different material to that of the sample being studied, a separate normalisation run is needed with identical operating conditions to obtain the ratio  $A_R/A_{R'}$ . In the neutron energy range 10 to 100 keV, resonances in Pb ( $E_R = 41.5$  keV,  $\Gamma_\gamma = 5.5$  eV,  $\Gamma_n = 1100$  eV,  $I_{\gamma 0} = 95\%$ ) (Allen and Macklin 1970a, Bird et al. 1973) or Al ( $E_R = 34.7$  keV,  $\Gamma_\gamma = 8.30$  eV,  $\Gamma_n = 3.42$  keV,  $I_{\gamma 0} = 60\%$ ) (Singh et al. 1971, Bird et al. 1973) are suitable for use for normalisation.

### 2. The use of a neutron flux monitor and measured detection efficiencies:

$$\sigma_{\gamma ij} = Y_{ij} / n \phi_j \epsilon_i a_i$$

where  $Y_{ij}$  is the observed yield and

$\phi_j$  the corresponding neutron flux for the  $j^{\text{th}}$  time of flight channel.

## 3. RESULTS AND DISCUSSION

### 3.1 Titanium

Figure 4 shows relative cross sections as a function of neutron energy for various pulse height intervals. These are respectively 7.9 to 9.4, 7.35 to 7.9, 6.6 to 7.0 and 6.25 to 6.6 MeV. The binding energies of  $^{48}\text{Ti} + n$  (73 per cent abundant) and  $^{47}\text{Ti} + n$  (7.9 per cent abundant) are respectively, 8.146 and 10.621 MeV. Previous work with a Ge(Li) detector (Broomhall 1972b) has shown a transition to the  $7/2^-$  ground state of  $^{48}\text{Ti}$  at a neutron energy of about 39 keV, implying a d-wave resonance. This resonance is clearly seen in Figures 4(a) and 4(b) at a neutron energy of 39.6 keV. Since the  $\gamma$ -ray energy range includes the ground state transition but no other state,

this is further evidence for the  $7/2^-$  transition which is presumed to be E1 after a d-wave resonance. Other resonances in these spectra are most probably due to capture by  $^{47}\text{Ti}$  (Ernst et al. 1970).

The 39.6 keV resonance is also apparent in Figure 4(c) corresponding to a transition to the  $3/2^-$  first excited state in  $^{49}\text{Ti}$ . The strength of this transition is consistent with a d-wave assignment for the 39.6 keV resonance.

In Figure 4(c), transitions to the first excited state of  $^{49}\text{Ti}$  are the main contributors and in Figure 4(d) the first, third and fifth contribute. An s-wave resonance at 37 keV gives a strong transition to the first excited state ( $3/2^-$ ), but only very weak transitions to other states. The broad s-wave resonance at 17 keV ( $\Gamma_n \approx 7.5$  keV) is the main feature of the spectrum. Table 2 summarises the data obtained in this experiment, total capture measurements (Allen and Macklin 1970 b) and transmission experiments (Goldberg et al. 1966). The peak structure of Figure 4(c) and 4(d) shows that even though the neutron energy range extends from 5 to 60 keV, approximately 70 per cent of all capture events are in the energy range 5 to 20 keV.

The experimental data show a small unexplained dip at 18 keV. Since the line shape of the detector is known at various energies, it is possible to subtract the contribution of  $\gamma_1$  and  $\gamma_3$  from the spectrum shown in Figure 4(d), leaving only the contribution of  $\gamma_6$ . The result is shown in Figure 5 for neutron energies up to 22 keV. The structure at 18 keV is evident in Figure 5 and has the form which could arise from level-level interference in partial capture cross sections. The feasibility of such measurements is therefore demonstrated, but the origin of the structure in Figure 5 requires further detailed investigation.

### 3.2 Iron

There are about ten resonances for capture by  $^{56}\text{Fe}$  in the energy range 10 to 60 keV (Hockenbury et al. 1969) and since the ground and first excited states of  $^{56}\text{Fe}$  are only 14 keV apart, capture spectra produce a significant number of gamma rays differing in energy by only a few keV. Measurements have been made using Ge(Li) detectors (Allen et al. 1969, Kenny 1971) and almost two thirds of all transitions are found to occur to the ground and first excited state doublet (although there are strong fluctuations from resonance to resonance).

Figure 6 shows relative cross sections as a function of neutron energy for four different pulse height intervals 7.5 to 7.8, 6.0 to 7.5, 5.66 to 6.0 and 4.3 to 5.66 MeV. Hockenbury (1969) reports resonances at 27.7, 34.1, 36.6, 38.3, 45.8, 51.9, 53.3 and 59.0 keV, in a total capture experiment. In the present experiment, the timing resolution (2.7 ns/m) enabled all these resonances to be resolved and they appear in one or more of the spectra of Figure 6 with energies which agree with Hockenbury's values to within a fraction of a kilovolt. The broad s-wave resonance at 27.7 keV and the sharper one at 34.1 keV occur in all spectra.

One feature of the previous Ge(Li) data (Kenny 1971) is the clear indication of transitions to  $5/2^-$  states at 135 and 706 keV excitation for neutron energies near 27, 37 and 52 keV. It has been argued (Bird et al. 1969) that these transitions result from capture of neutrons with  $\ell_n \geq 1$ , since  $\ell_n = 0$  could only lead to these states by M2 transitions. Since the 27.7 keV resonance is assigned as s-wave, the implication is that there may be a weak neighbouring resonance with  $\ell_n \neq 0$ . It could be argued that the spectrum in Figure 5(c) is double peaked at energies 27.4 and 27.7 keV, but statistical errors and timing uncertainties do not justify definite allocation of two resonances. It has also been argued (Jackson and Strait 1971) that the 34.1 keV resonance is p-wave. If this is so, then there are M1 transitions present to  $1/2^-$ ,  $3/2^-$  and  $5/2^-$  final states. The Ge(Li) data (Kenny 1971) confirm that transitions occur to all these states, but the data do not allow the multipolarity to be determined. Table 3 summarises the resonance energies observed in this experiment and also includes data from Goldberg et al. (1966) and Hockenbury et al. (1969) for comparison.

### 3.3 Nickel

As with iron and titanium, Ge(Li) spectra for keV capture in nickel are available (Allen et al. 1969, Bird et al. 1973), but information on individual resonances is restricted. The dominant isotope in nickel is  $^{58}\text{Ni}$  which is 68 per cent abundant. Its average cross section near 30 keV is two or three times that for the other isotopes ( $^{60}\text{Ni}$  and  $^{62}\text{Ni}$ ) and the binding energy is 9 MeV for  $^{58}\text{Ni} + n$ , compared with 7.8 and 6.8 MeV respectively for the other two. Hence discussion can be restricted largely to  $^{58}\text{Ni} + n$ .

Figure 7 shows relative cross sections as a function of neutron energy for four different pulse height intervals: 8.7 to 9.4, 8.0 to 8.7, 7.36 to 8.0 and 2.5 to 7.36 MeV. Figure 7(a) has an approximate cross section scale obtained by assuming values of the resonance parameters for the 15.5 keV resonance ( $\Gamma_\gamma = 0.6$  eV,  $\Gamma_n = 1.5$  keV,  $I_{\gamma 0} = 19$  per cent).

The total cross section for  $^{58}\text{Ni}$  shows two strong s-wave resonances at 15.5 and 63.6 keV (Goldberg et al. 1966). However, as for other elements, e.g. Ti and Fe, many more resonances are observed in the capture cross section. Table 4 summarises the resonances in  $^{58}\text{Ni}$  as observed in this experiment and elsewhere (Hockenbury et al. 1969 and Ernst et al. 1970).

### 3.4 Lead

Lead shows somewhat different behaviour from the other nuclei in that there is a broad s-wave resonance for  $^{207}\text{Pb} + n$  (22.6 per cent abundant) at 41.5 keV and only small resonances have been reported at other energies. The 41.5 keV resonance has a neutron width of 1100 eV, a radiation width ( $\Gamma_\gamma$ ) of 5.5 eV and  $J^\pi = 1^-$  (Allen and Macklin 1970a). Spectra from this resonance (Bird et al. 1973) show that transitions to the  $0^+$  ground state account for 95 per cent of all observed decays from the resonance. From multipolarity considerations it is expected that  $\sigma_{\gamma 0}$  will show predominantly the 41.5 keV resonance, but p-wave resonances will contribute appreciably to  $\sigma_{\gamma 1}$ .

The relative cross section as a function of neutron energy is shown in Figure 8 for the ground state gamma ray transition. Resonances are observed at 30.0, 35.2, 37.5, 40.9 and 48.8 keV for  $\gamma$ -rays between 7.07 and 7.44 MeV, so no other isotopes should be included. These are in fairly good agreement with recent high resolution total capture measurements of Allen and Macklin (1971) who give values of 30.5, 33.0, 37.8, 41.2 and 48.5 keV. A small resonance has been observed at 35 keV in the  $(\gamma, n)$  reaction (Bowman et al. 1969).

## 4. CONCLUSIONS

A large volume well shielded NaI detector can be used in conjunction with a pulsed Van de Graaff accelerator to measure partial capture cross sections in the energy range 10 to 100 keV. Count rates are sufficient to allow the use of thin targets so multiple scattering effects are minimised. In some cases, resonances separated in energy by one kilovolt can be resolved.

The nuclei chosen for study were those with strong high energy transitions and widely spaced resonances. Single resonances were observed for individual transitions in  $^{48}\text{Ti}$ ,  $^{56}\text{Fe}$ ,  $^{58}\text{Ni}$  and  $^{208}\text{Pb}$ . Resonances at 17 keV in  $^{48}\text{Ti}$ , 15.5 keV in  $^{58}\text{Ni}$  and 27.8 keV in  $^{56}\text{Fe}$  dominate the capture cross sections for high energy transitions to  $3/2^-$  and  $1/2^-$  final states. These resonances also dominate the scattering cross sections. Further evidence is obtained for a resonance at 39.6 keV in  $^{48}\text{Ti}$  which shows transitions to  $7/2^-$  and  $3/2^-$  final states as would be expected for a  $5/2^-$  d-wave resonance.

Although some estimates were obtained of the high energy transition strengths for the smaller resonances in  $^{56}\text{Fe}$  and  $^{58}\text{Ni}$  (assigned as p-wave by other workers), no additional information on their  $\ell$ -wave character can be advanced. The Ge(Li) spectra for iron suggest that there may be a higher  $\ell$ -wave resonance near 27 keV, but the time of flight spectra show that if such a resonance exists, it is very small.

## 5. REFERENCES

- Allen, B.J., Bird, J.R. and Kenny, M.J. (1969) – AAEC/E200.
- Allen, B.J. and Macklin, R.L. (1970a) – Phys. Rev. Lett. 25, 1675.
- Allen, B.J. and Macklin, R.L. (1970b) – Bull. Am. Phys. Soc. 15, 1667.
- Allen, B.J. and Macklin, R.L. (1971) – Proc. 3rd Conf. on Neutron Cross Sections and Technology, Knoxville, Tennessee, 764.
- Bird, J.R., Allen, B.J. and Kenny, M.J. (1969) – Phys. Lett. 27B, 638.
- Bird, J.R., Allen, B.J., Bergqvist, I. and Biggerstaff, J.A. (1973) – Nuclear Data A11, 6.
- Bowman, C.D., Baglan, R.J. and Berman, B.L. (1969) – Phys. Rev. Lett. 23, 796.
- Broomhall, G.J. (1971) – AAEC/TM603.
- Broomhall, G.J. (1972a) – Ph. D. Thesis, University of Melbourne (unpublished).
- Broomhall, G.J. (1972b) – Aust. J. Phys. 25, 9.
- Clancy, B.E. (1969) – AAEC/TM505.
- Ernst, E.R., Frohner, F.H. and Kompe, D. (1970) – Karlsruhe Report KFK1231.
- Goldberg, M.D., Mughabghab, S.F., Magurno, B.A. and May, V.M. (1966) – Brookhaven National Laboratory report BNL325, 2nd Ed. Supp. No. 2.
- Hockenbury, R.W., Bartolome, Z.M., Tatarczuk, J.R., Moyer, W.F. and Block, R.C. (1969) – Phys. Rev. 178, 1746.
- Jackson, H.E. and Strait, K.N. (1971) – Phys. Rev. C4, 1314.
- Kenny, M.J. (1971) – Aust. J. Phys. 24, 805.
- Singh, U.N., Garg, J.B., Rainwater, J., Havens Jr. W.W., Wynchank, S., Slagowitz, M. and Llov, H. (1971) – Proc. Int. Conf. on Statistical Properties of Nuclei, Albany. Plenum Press, p.81.

TABLE 1

DETAILS OF TARGET MATERIALS AND RUNNING CONDITIONS

Target (natural element)	Thickness (atom/barn)	Mass (g)	Flight Path (m)	Time Resolution (ns/m)
Ti	0.006	45.4	1.00	4.0
	0.012	90.8	1.00	4.0
Fe	0.013	498	1.50	2.7
Ni	0.010	134	0.63	4.7
Pb	0.008	207	1.00	4.0

TABLE 2

RESONANCES IN  $^{46}\text{Ti}(n,\gamma)^{46}\text{Ti}$

$E_R$ (keV)		$\Gamma_n$ (keV)	$E_R(\gamma_0)$	$E_R(\gamma_1)$	$E_R(\gamma_6)$
Allen & Macklin (1970b)	Goldberg et al. (1966)	Goldberg et al. (1966)	This Experiment		
11.4	—	—	—	11.4	—
13.4	—	—	—	—	13.4
(17)	17.3	7.5	—	17.0	17.0
—	—	—	—	—	18.2
21.6	—	—	—	—	—
22.0	22.0	0.5	—	22.1	22.1
24.1	—	—	—	24.1	24.1
37.0	37.0	1.1	—	37.0	(very small)
39.2	—	—	39.6	39.6	—
42.2	—	—	—	—	42.1

**TABLE 3**  
**RESONANCES in  $^{56}\text{Fe}(n,\gamma)^{57}\text{Fe}$**

$E_R$ (keV)	$\Gamma_n$ (eV)	$\sigma_0\Gamma_\gamma$ (b.eV)	$\Gamma_\gamma$ (eV)	$E_R$ (keV)	$E_R$ (keV)
Goldberg et al. (1966) Hockenbury et al. (1969)				This Work All $\gamma$ -rays	Work $\gamma_0, \gamma_1$ Only
22.7	10	21.9	—	—	—
—	—	—	—	27.4	—
27.7	1600		1.4	27.9	27.7
34.1	—	44.1	—	34.2	34.2
36.6	10	21.4		36.6	36.6
38.3	—	30.1	—	38.3	38.3
45.8	—	18.7	—	45.9	—
51.9	—	25.6	—	52.0	52.0
					(very small)
53.3	—	26.4	—	53.4	—
55.0	—	6.7	—	—	
59.0	—	24.2	—		
63.1					

**TABLE 4**  
**RESONANCES IN  $^{58}\text{Ni}(n,\gamma)^{59}\text{Ni}$**

$E_R$ (keV)	$\sigma_0\Gamma_\gamma$ (b.eV)	$E_R$ (keV)	$E_R$ (keV) ( $\gamma_0$ )	$\sigma_0\Gamma_{\gamma_0}$ (b.eV)	$E_R$ (keV) ( $\gamma_0, \gamma_1, \gamma_2, \gamma_3$ )
Hockenbury et al. (1969)		Ernst et al. (1970)	This Work		
13.3	63.2	13.3	—		13.2
13.6	101	13.7	—		
(14–16)	—	(15.4)	15.1	105	15.1
19	8.7	—	—	—	18.7
20	26.0	20	19.8	7	19.8
21.1	70	21.2	—	—	21.0
—		26.0	—	—	26.0
26.6	68	26.6	26.6	10	26.6
32.4	114	32.3	32.3	54	32.3
34.2	49.5	34.2	34.1	6	34.1
36.1	62	36.2	36.1	23	36.1
39.5	—	39.6	—	—	39.5
47.9	87.5	47.6	47.9	6	47.9
52.1	—	52.2	52.0	11	52.0
54.8	16.2	54.6	54.6	—	54.6
		57.9			
60.1	—	60.0	60.0	—	60.0
61.8	—	61.9	61.8	—	61.8



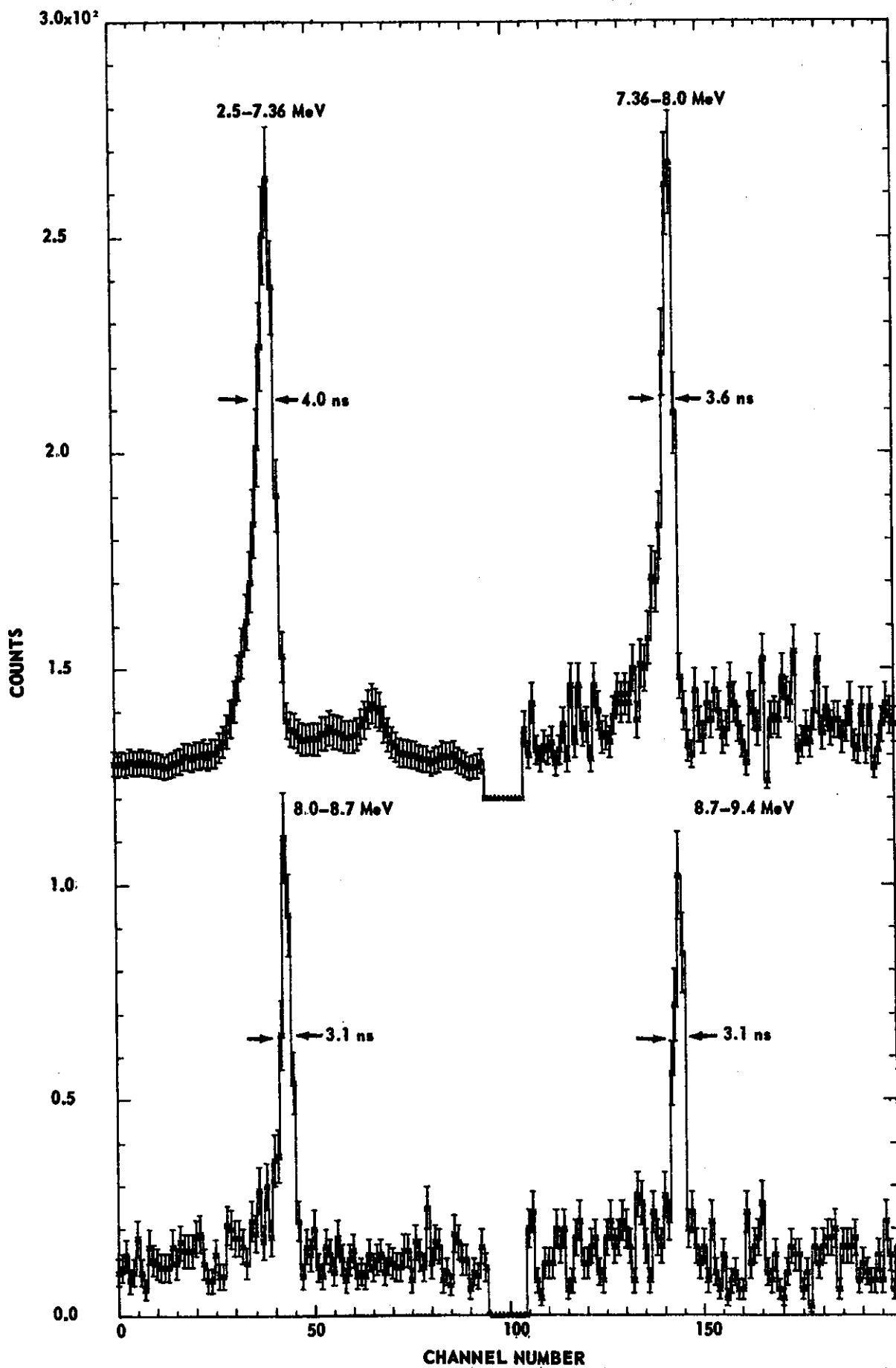


FIGURE 1. TIME RESOLUTION OF PROMPT GAMMA PEAK FOR FOUR PULSE HEIGHT RANGES

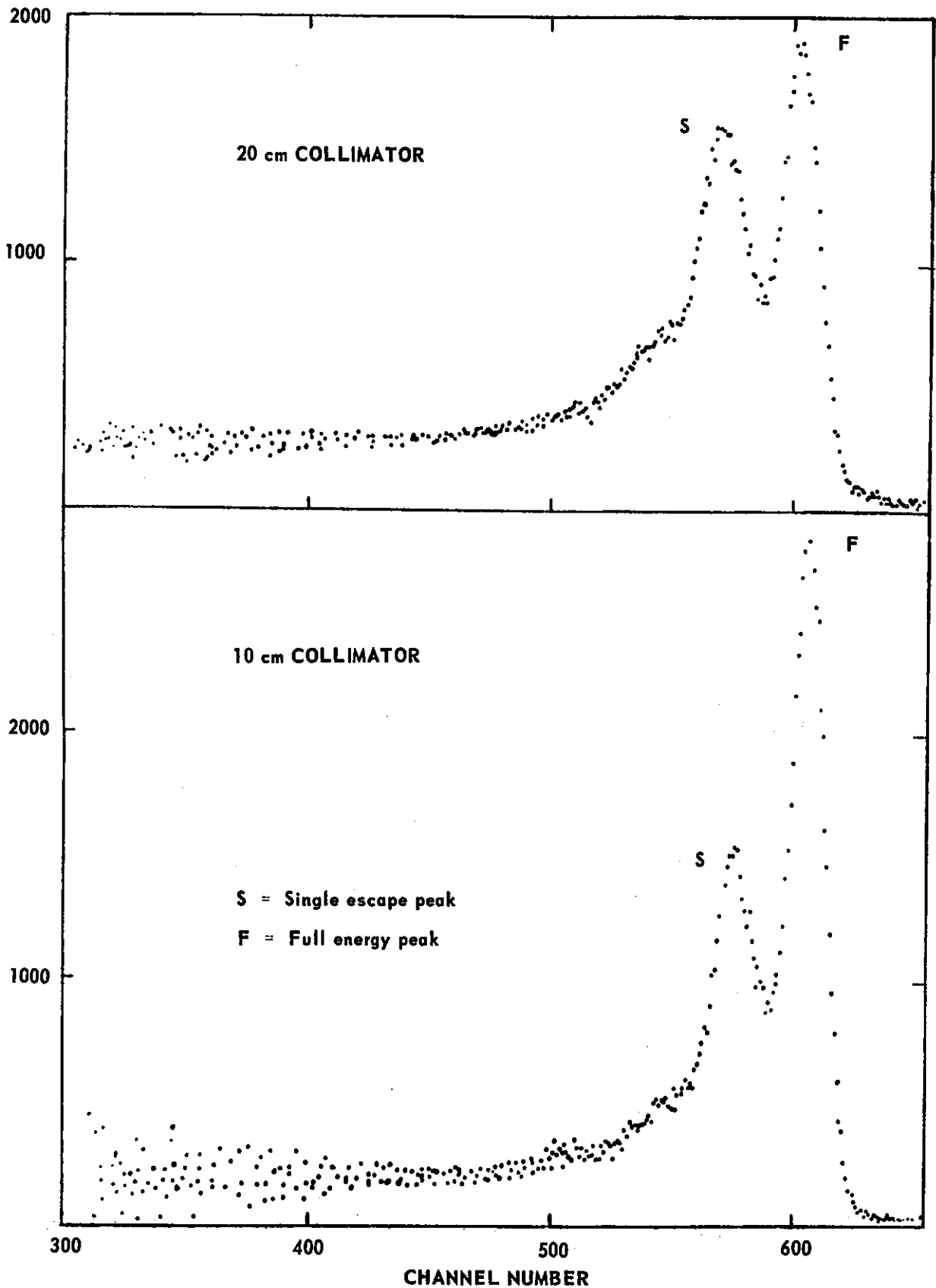


FIGURE 2. NaI DETECTOR RESPONSE FUNCTIONS FOR A 9.94 MeV GAMMA RAY

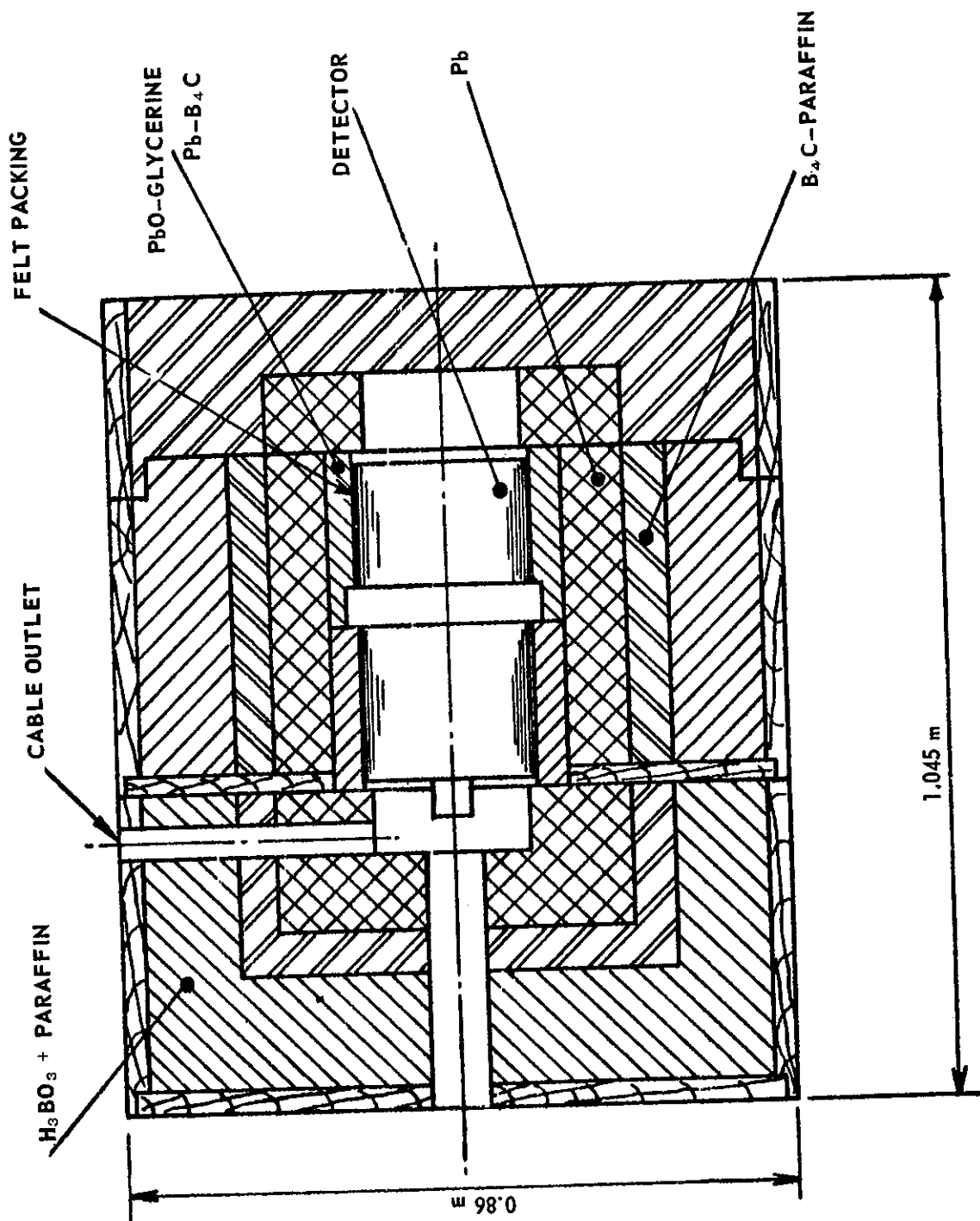


FIGURE 3. DETECTOR SHIELDING ASSEMBLY (LONGITUDINAL SECTION)

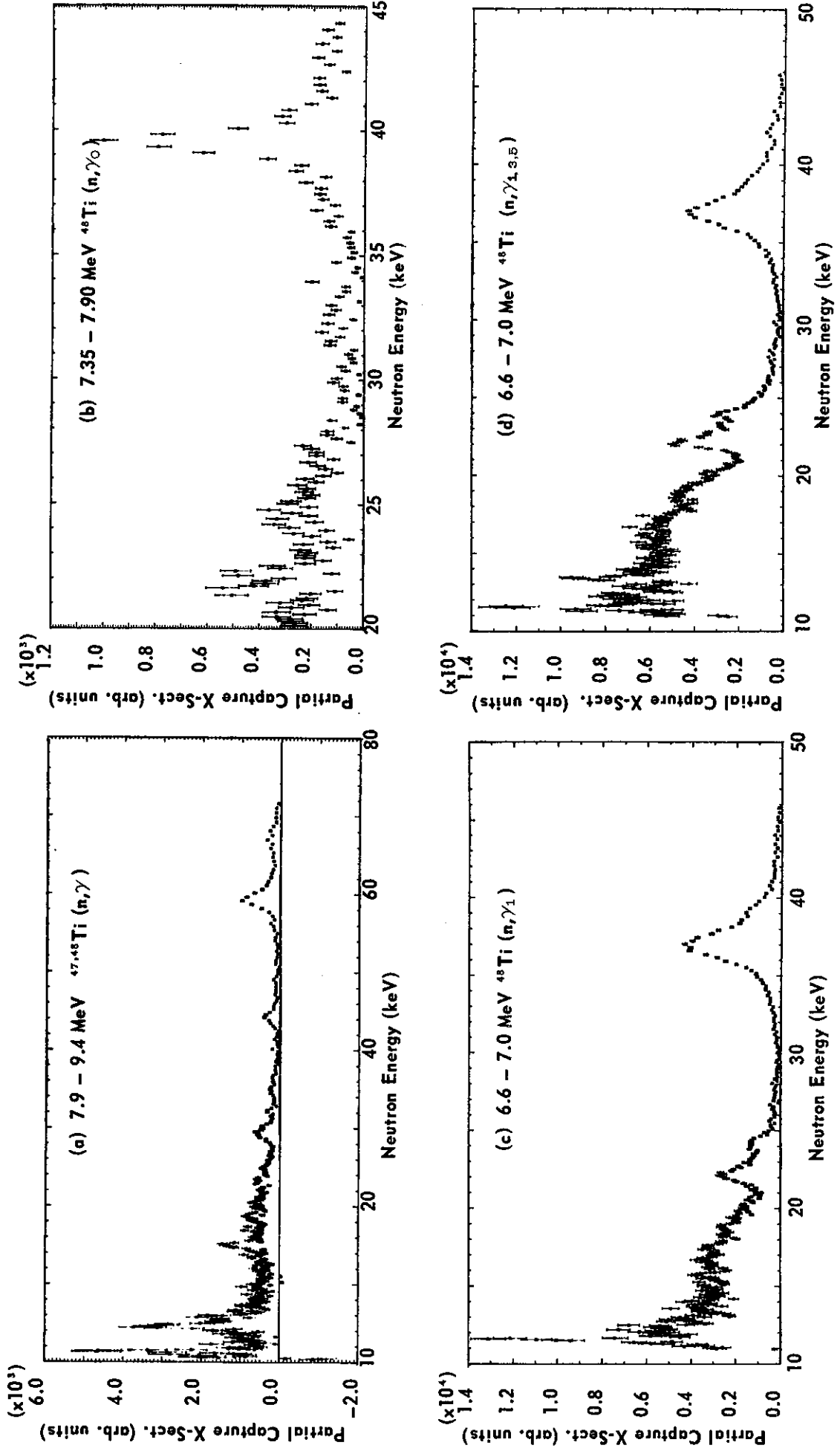


FIGURE 4. RELATIVE PARTIAL CAPTURE CROSS SECTIONS FOR CAPTURE BY  $^{47}\text{Ti}$  AND  $^{48}\text{Ti}$  USING A 1.00 m FLIGHT PATH FOR VARIOUS PULSE HEIGHT INTERVALS

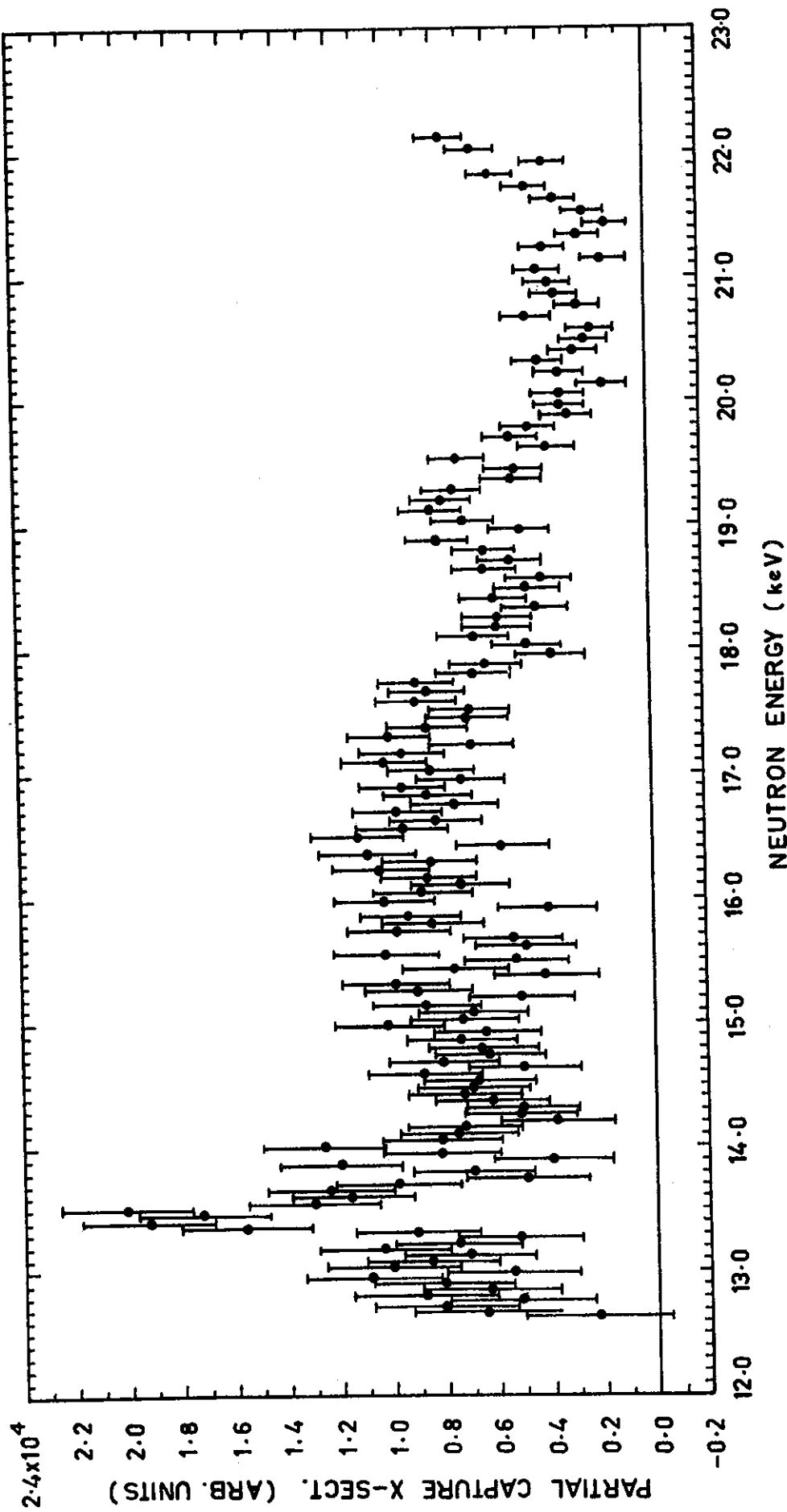


FIGURE 5. RELATIVE PARTIAL CAPTURE CROSS SECTION FOR CAPTURE BY  $^{48}\text{Ti}$  BETWEEN 12 AND 23 keV USING A 1.00 m FLIGHT PATH

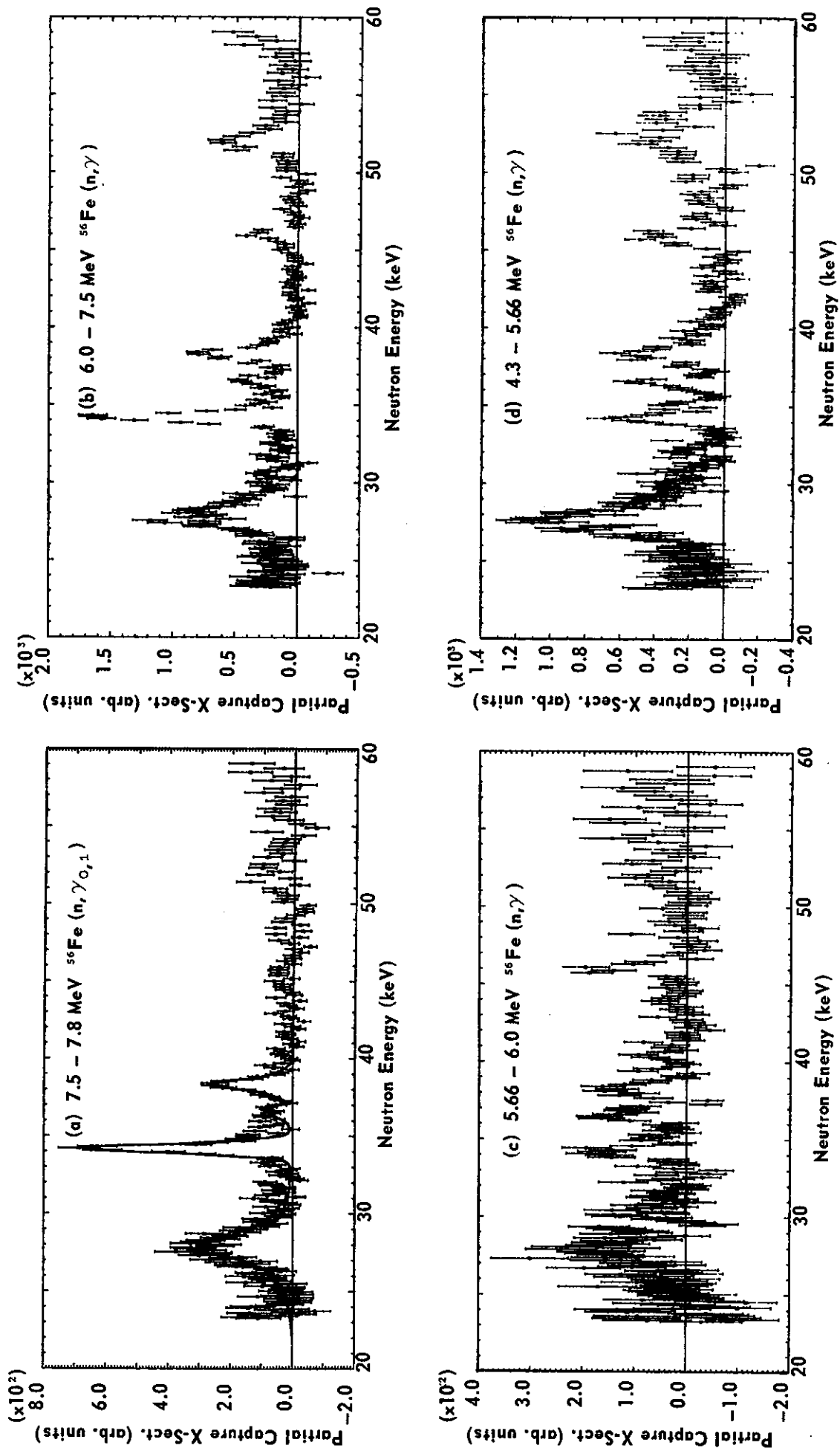


FIGURE 6. RELATIVE PARTIAL CAPTURE CROSS SECTIONS FOR CAPTURE BY IRON USING A 1.50 m FLIGHT PATH FOR VARIOUS PULSE HEIGHT INTERVALS

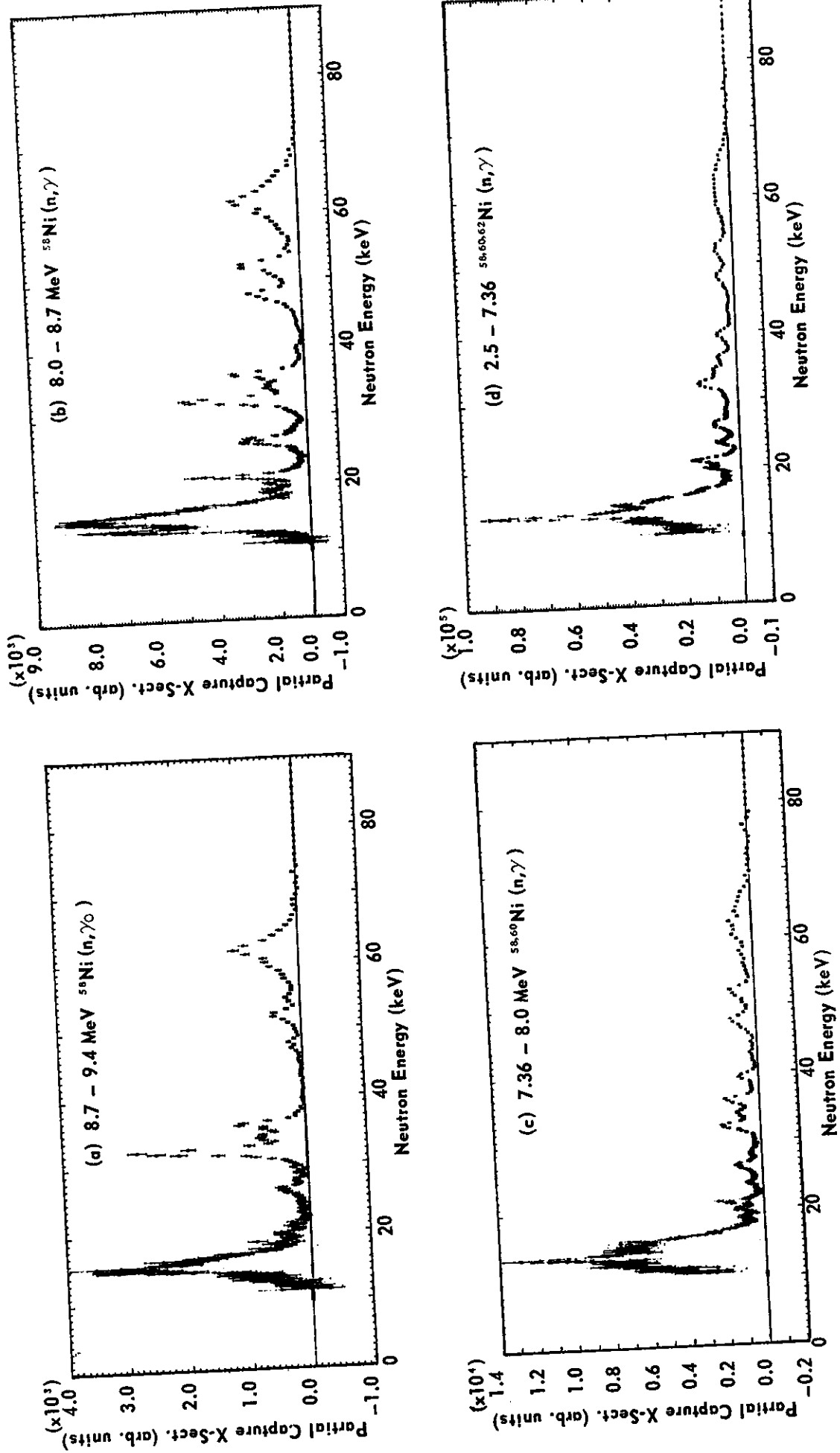


FIGURE 7. RELATIVE PARTIAL CAPTURE CROSS SECTIONS FOR CAPTURE BY NICKEL USING  
A 0.63 m FLIGHT PATH FOR VARIOUS PULSE HEIGHT INTERVALS

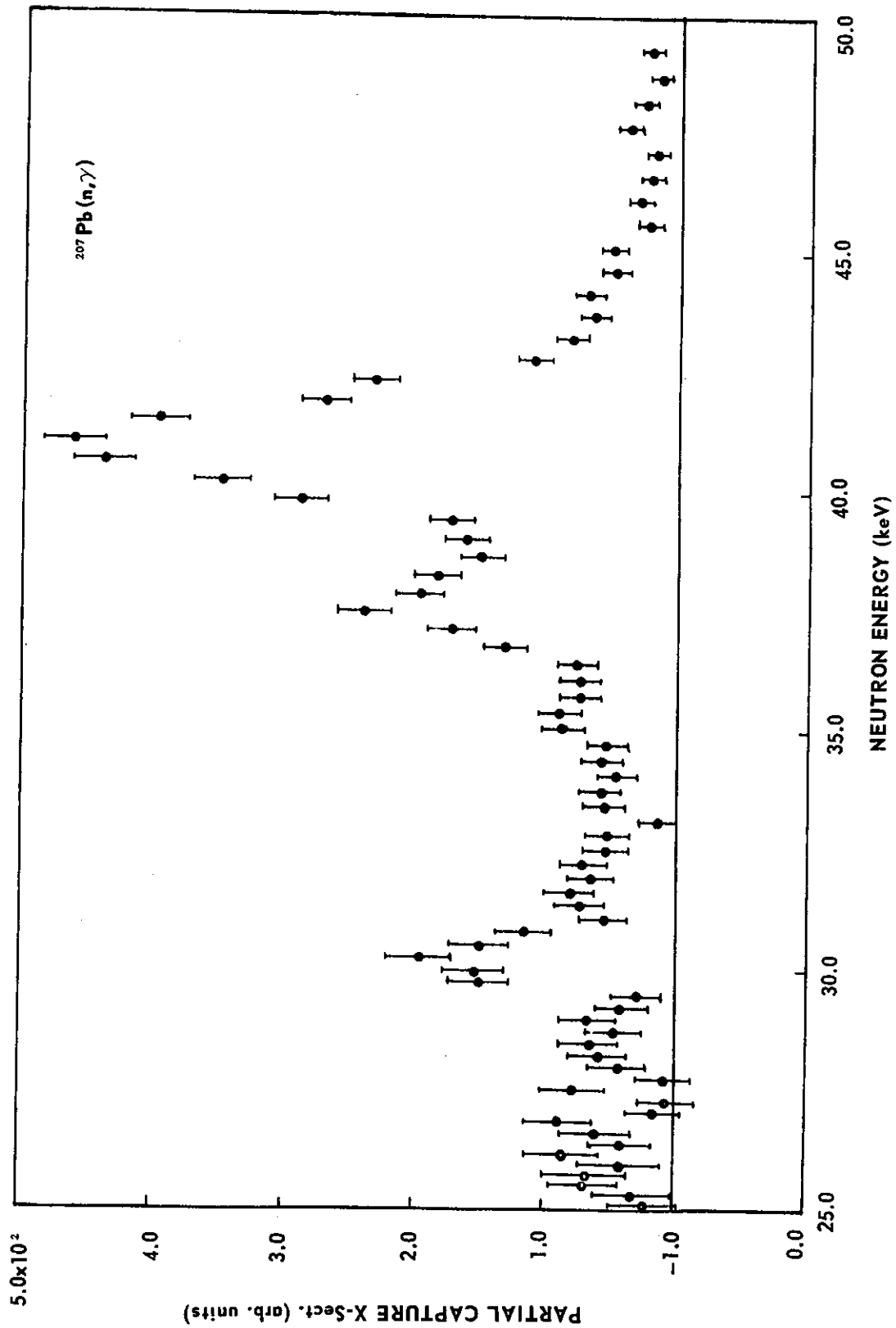


FIGURE 8. CAPTURE CROSS SECTION FOR THE GROUND STATE TRANSITION FOLLOWING CAPTURE BY  $^{207}\text{Pb}$  USING A 1.00 m FLIGHT PATH